RESEARCH PAPER

Enhancement of Mechanical and Durability Properties of Recycled Aggregate Concrete Through Partial Cement Replacement With Marble Dust and Finely Ground Recycled Glass Dust: Experimental Investigation and Machine Learning-Based Predictive Modelling

Sonar Vaishnavi Mahendra[1], Sachin U. Pagar[2], Ketan A. Salunke[3]

[1]P.G Scholar, Department of Civil Engineering, Late G. N. Sapkal College of Engineering, Savitribai Phule Pune University, Nashik 422 213, Maharashtra, India

Email: vaishnavi.sonar@gnsce.edu.in

[2]Assistant Professor, Department of Civil Engineering, Late G. N. Sapkal College of Engineering, Savitribai Phule Pune University, Nashik 422 213, Maharashtra, India

[3]Professor & Head, Department of Civil Engineering, Late G. N. Sapkal College of Engineering, Savitribai Phule Pune University, Nashik 422 213, Maharashtra, India

Received: 17th Mar, 2026 | Revised: 29th Mar, 2026 | Accepted: 19th Apr, 2026 | Available Online: 5th May, 2026

ABSTRACT

The escalating generation of construction and demolition (C&D) waste and the environmental burden imposed by Portland cement production have collectively intensified global interest in recycled aggregate concrete (RAC) as a sustainable structural material. However, RAC inherently exhibits inferior mechanical performance relative to conventional concrete, primarily because of the elevated porosity and compromised interfacial transition zone (ITZ) introduced by residual adhered mortar on recycled aggregate surfaces. This study addresses these limitations through a combined experimental and machine-learning investigation of RAC in which ordinary Portland cement (OPC 53-grade) was partially replaced with marble dust (MD) and finely ground recycled glass dust (GD) — both sized at 70 µm — at total replacement levels of 0% (control M1), 10% (M2), 15% (M3), and 20% (M4), with concomitant introduction of recycled coarse aggregate (RCA) at 0%, 20%, 40%, and 60%. Four mix variants conforming to M30 design strength were cast per IS 10262:2019; compressive strength (3, 7, 14, 28 days), split tensile strength (7, 28 days), flexural strength (7, 28 days), and water absorption were systematically evaluated. The 20% MD+GD blend (M4) achieved a 28-day compressive strength of 35.40 MPa — a 24.5% improvement over the control (28.43 MPa) — while split tensile and flexural strength increased by 55.7% and 50.6%, respectively. Water absorption showed a nuanced response consistent with the competing effects of RCA porosity and pozzolanic pore refinement. The mechanistic basis for these improvements is attributed to dual co-operative phenomena: pozzolanic reactivity of glass dust generating additional C-S-H gel, and the physical micro-filling action of marble dust that densifies the concrete matrix and strengthens the ITZ. To extend predictive capability across an expanded compositional space, an artificial neural network (ANN) with a 7-14-10-14-5 multi-output architecture was developed, achieving R^2 values of 0.984 and 0.980 for compressive and flexural strength prediction on the held-out test set, outperforming Random Forest, XGBoost, and SVR baselines. SHAP-based feature importance analysis confirmed that RCA replacement percentage and glass dust content are the dominant predictors of all five output responses.

Keywords: Recycled Aggregate Concrete; Marble Dust; Recycled Glass Dust; Supplementary Cementitious Material; Compressive Strength; Durability; Interfacial Transition Zone; Artificial Neural Network; Shap; Sustainable Construction

How to cite this article: Mahendra S V, Pagar S U, Salunke K A., Enhancement of Mechanical and Durability Properties of Recycled Aggregate Concrete Through Partial Cement Replacement With Marble Dust and Finely Ground Recycled Glass Dust: Experimental Investigation and Machine Learning-Based Predictive Modelling. Int J Drug Deliv Technol. 2026;16(43s): 1009-1026; Doi: 10.25258/Ijddt.16.43s.107

1. INTRODUCTION

Concrete is the single most consumed manufactured material on Earth, with annual production exceeding 30 billion tonnes, a demand driven by accelerating urbanisation in Asia, Africa, and Latin America [1]. This scale of production carries a commensurate environmental cost: the manufacture of ordinary Portland cement alone contributes approximately 7–8% of global anthropogenic CO_2 emissions, while the quarrying of natural aggregates degrades river systems, hillsides, and ecologically sensitive terrain at an irreversible pace [2]. Simultaneously, the construction and demolition (C&D) sector worldwide generates over 3.5 billion tonnes of waste annually, the majority of which is either stockpiled or landfilled, constituting a significant misallocation of recoverable material resources [3].

Recycled aggregate concrete (RAC) in which virgin coarse aggregate is partly or fully substituted by crushed demolition concrete presents a structurally and environmentally credible pathway toward resource circularity in the construction sector. However, the technical case for RAC is complicated by its characteristically inferior mechanical performance: the residual adhered mortar encrusting recycled aggregate surfaces introduces additional porosity, reduces aggregate specific gravity, and creates a double interfacial transition zone (ITZ) between new paste and old mortar, and between old mortar and original aggregate each representing a locus of structural weakness [4]. Published literature consistently reports 10–30% reductions in compressive strength and commensurate increases in creep, shrinkage, and water absorption relative to conventional concrete at equivalent replacement levels.

Two industrial by-products have attracted research attention as partial cement replacements capable of compensating for these deficiencies. Marble dust (MD), generated in quantities estimated at 15% of total marble processed in stone-cutting operations, is an inert calcium-carbonate-rich powder whose particle size typically comparable to or finer than cement endows it with a micro-filling function that physically densifies the cement matrix and refines the ITZ microstructure [5,6]. Finely ground recycled glass dust (GD), derived from milling waste glass bottles and packaging to sub-100 µm particle sizes, possesses a high amorphous silica (SiO_2) content that confers genuine pozzolanic reactivity: the secondary pozzolanic reaction between SiO_2 and calcium hydroxide ($Ca(OH)_2$) a by-product of cement hydration generates additional calcium silicate hydrate (C-S-H) gel, the principal strength-giving phase in hardened concrete [7,8].

Despite a growing body of individual studies on MD and GD as cementitious supplements, and a separate literature on RAC modification, the combined effect of simultaneously deploying MD and GD as binary cement replacement agents in RAC specifically the quantitative interaction between RCA replacement level, total dust content, and resulting mechanical and durability properties have not been comprehensively characterised. Furthermore, while machine learning (ML) approaches have been applied to predict compressive strength of plain cement concrete with increasing sophistication, multi-output ML modelling of RAC incorporating dual supplementary cementitious materials, supported by SHAP-based explainability, remains essentially unexplored [9,10].

The present investigation addresses these gaps through four coordinated objectives: (i) systematic experimental characterisation of M30-grade RAC at four MD+GD replacement levels and four RCA substitution levels; (ii) mechanistic interpretation of all observed property changes through reference to pozzolanic chemistry, micro-filling theory, and ITZ physics; (iii) development and validation of a multi-output ANN model for simultaneous prediction of five concrete properties; and (iv) SHAP-based quantification of the relative influence of seven mix variables on each property output, enabling physically grounded model interpretation.

2. STATE OF THE ART

2.1 Marble Dust as a Supplementary Cementitious Material

Özkılıç [11] conducted a systematic experimental programme on concrete where waste marble powder (WMP) replaced cement at incremental levels and demonstrated that compressive strength, flexural strength, and durability metrics (water absorption, chloride permeability) were optimised at WMP content of approximately 10–15% by mass of cement. Beyond this threshold, dilution of the cementitious phase outweighed micro-filling benefits, producing a net reduction in mechanical performance. Abbas et al. [12] corroborated these findings in a 2025 study providing microstructural evidence via mercury intrusion porosimetry and SEM imaging for a reduction in cumulative pore volume and a refinement of pore size distribution at 10–15% WMP replacement. Kuoribo et al. [13] reviewed 60+ published studies and concluded that marble dust acts predominantly as a physical micro-

filler rather than a chemically reactive SCM, with benefits arising from improved particle packing density and reduced inter-particle void space. Ofuyatan et al. [14] extended this analysis to self-compacting concrete (SCC) incorporating recycled aggregates, finding that WMP at 5–10% partially compensated for the fresh-state and hardened-state drawbacks of RA by improving bulk density and ITZ quality.

Early investigations into the use of alumina silicate in self-consolidating concrete indicated that such additions can improve the strength of the concrete during both the setting and hardening phases [1]. Additional investigations into the use of such materials in self-flowing concrete in the presence of elevated temperatures indicated that such additives can lead to improvements in the remaining strength of that concrete after exposure to those temperatures [2]. Research into 3D printing techniques indicated that it is possible to print concrete elements, but that some of the properties of the concrete are often reduced in such construction techniques [3]. The inclusion of polypropylene geo-fabric into concrete has been shown to lead to improvements in crack control and crack resistance of that concrete [4].

The use of both steel fibers and polypropylene geo-fabric in concrete has been shown to lead to improvements in the strength of that concrete, as well as to the crack resistance of that concrete [5]. Investigations into pervious concrete revealed methods of creating pervious concrete that exhibited improved strength [6]. The addition of steel scrap to concrete has been shown to improve the strength of that concrete [7]. Additionally, research into the replacement of fine aggregate with rice husk ash indicates that such a replacement is one means of developing sustainable construction materials [8]. Further investigations into the use of waste steel within concrete indicated that the use of steel scrap to strengthen concrete can lead to improvements in the strength and toughness of those construction materials [9]. Investigations into the addition of nano-fillers to concrete indicate that concrete with nano-fillers exhibit improvements in their reliability and strength [10]. Additionally, studies of geopolymer concrete that are reinforced with both steel and polypropylene fibers indicate that these materials can improve the ductility of those geopolymer concrete [11]. The development of affordable 3-axis concrete printers was found to be useful in the construction of sustainable housing systems [12].

In the construction of concrete that utilize recycled aggregates, the addition of polyacrylate-based super absorbent polymers indicated improvements in strength of that concrete [13]. Additionally, investigations into the use of bio-mediated methods for the remediation of cracked concrete indicate that such methods can be effective in increasing the durability of those construction materials [14]. Studies of the use of waste foundry sand within concrete indicated that such sand could lead to improvements in the strength, durability, and other physical properties of concrete [15]. Additionally, investigations into the development of self-curing concrete that utilizes polyethylene glycol and recycled PET indicated that such concrete have the potential to reduce the scarcity of water for construction purposes [16].

These investigations into concrete indicate the use of supplementary cementitious materials [1], thermally-resistant modified concrete [2], digital construction technologies [3], crack-control materials like polypropylene geo-fabric [4], methods that incorporate both steel and polypropylene fiber to provide additional strength and crack control to concrete [5], pervious concrete [6], concrete that incorporate recycled metallic waste [7], construction materials that utilize agricultural by-products [8], methods of utilizing waste steel to enhance the strength and toughness of concrete [9], nano-scale additives to improve the strength of concrete [10], geopolymer concrete that utilize both steel and polypropylene fibers [11], 3D printing methods to construct sustainable housing [12], internal curing techniques to improve the strength of concrete that utilize recycled aggregates [13], bio-based methods to remediate concrete [14], methods of utilizing waste foundry sand in concrete [15], and self-curing concrete comprised of sustainable composite materials [16]. Thus, each of these methods and technologies redefines concrete construction materials that are both strong and sustainable.

2.2 Recycled Glass Dust as a Pozzolanic SCM

Muhedin et al. [15] demonstrated that waste glass powder (WGP) at 10–20% cement replacement achieved improved later-age compressive strength and reduced chloride permeability through confirmed pozzolanic reaction between SiO_2 and $Ca(OH)_2$. The onset of meaningful pozzolanic reactivity at 28 days rather than 7 days explains the characteristic pattern of modest early-age strength followed by pronounced late-age gains that

have been consistently reported in the glass dust literature [16]. Olabimtan et al. [17] combined GD with recycled fine aggregate and established that GD-modified mixes exhibited improved mechanical properties and durability indices despite workability reductions at high GD content. Karalar et al. [18] scaled these observations to structural level, demonstrating improved flexural capacity and post-cracking behaviour in RAC beams incorporating GD at 10–20% cement replacement.

2.3 Combined RAC with Marble and Glass Dust

Zhou et al. [19] comprehensively reviewed waste glass applications in concrete and identified that (a) sufficiently fine glass powder (<75 µm) suppresses alkali-silica reaction (ASR) risk by reducing aggregate-scale glass particle mobility, (b) glass powder refines pore structure through its pozzolanic reaction product, and (c) combined use with RA offers potential to restore RAC durability when both materials are at appropriate dosages. Jhakal et al. [20] confirmed that practical mix modifications appropriate admixture dosing, pre-saturation of RCA can manage workability reductions when both wastes are co-deployed. Khan et al. [21] applied ML prediction to glass powder concrete and demonstrated that optimal GD replacement ranges are better identified through data-driven models than through trial-and-error experimental programmes.

2.4 Machine Learning in RAC Property Prediction

The application of artificial neural networks and gradient-boosted tree models to concrete strength prediction has expanded substantially. Khan et al. [21] achieved $R^2 \approx 0.96$ for compressive strength prediction of glass powder concrete using XGBoost. Golafshani et al. [22] demonstrated ANN superiority over empirical equations for RAC elastic modulus prediction, particularly in the presence of multi-component supplementary materials. Despite these advances, no published study has developed a validated multi-output ANN model simultaneously predicting compressive, tensile, flexural, and durability properties of RAC modified by binary MD+GD cement replacement, with SHAP-based feature importance attribution.

2.5 Research Gap

The reviewed literature establishes that: (1) MD and GD individually improve RAC properties at moderate replacement levels; (2) their combined deployment in RAC has not been quantitatively studied with full mechanical and durability characterisation; (3) ML-based prediction of RAC with binary SCMs is absent from the literature; and (4) no SHAP analysis has been applied to quantify the relative influence of MD and GD content alongside RCA level on multi-dimensional concrete performance. This study directly addresses all four gaps.

3. MATERIALS AND EXPERIMENTAL PROGRAMME

3.1 Research Methodology Overview

Figure 1. Research methodology flowchart: from material characterisation through experimental testing to ML model development and analysis.

3.2 Materials

3.2.1 Cementitious and Supplementary Materials

Ordinary Portland Cement (OPC) of 53-grade conforming to IS 12269:2013 was employed as the base binder. Physical properties were determined per IS 4031 (Parts 1–15): standard consistency 32%, specific gravity 3.04, and fineness (90-µm sieve residue) 4% well within the IS 12269 maximum of 10%. These values confirm that the cement is of normal hydration characteristics and adequate fineness for strength development.

Marble dust (MD) was sourced from a marble-processing stone yard in Nashik, Maharashtra. The material was air-classified to achieve a target particle size of 70 µm, consistent with published recommendations for micro-filling effectiveness [11]. XRF analysis confirmed $CaCO_3$ as the dominant phase (>92%), with minor SiO_2 and Al_2O_3 content, supporting its classification as a physically reactive micro-filler rather than a chemically reactive pozzolan. Market procurement rate: ₹189/kg.

Finely ground recycled glass dust (GD) was produced by crushing and ball-milling post-

consumer glass waste (principally clear bottles) to 70 µm fineness. XRF characterisation revealed SiO_2 content of approximately 71%, with Na_2O (13%) and CaO (9%) as secondary phases a composition consistent with soda-lime glass and sufficient amorphous silica content for pozzolanic activity at the particle sizes employed [7]. Market procurement rate: ₹85/kg.

3.2.2 Fine Aggregate

Natural river sand conforming to Zone II of IS 383:2016 was used. The fineness modulus was determined as 2.70 from sieve analysis on a 500 g sample (Table 1), with specific gravity 2.60 measured by pycnometer per IS 2386 Part III. All gradation results fell within Zone II envelope limits.

IS Sieve (mm)	Retained (g)	Cum. % Retained	Cum. % Passing	IS 383 Zone II (%)
4.75	12	2.40	97.60	90–100
2.36	17	5.80	94.20	75–100
1.18	80	21.80	78.20	55–90
0.600	156	53.00	47.00	35–59
0.300	172	87.40	12.60	8–30
0.150	59	99.20	0.80	0–10
Pan	4	100.0	0.0	

Table 1. Sieve analysis of fine aggregate (IS 2386 Pt I). FM = 2.70; Zone II grading confirmed.

3.2.3 Natural Coarse Aggregate (NCA)

Crushed granite of 20 mm nominal maximum size conforming to IS 383:2016 was used. Flakiness index (FI = 20.36%) and elongation index (EI = 20.16%) were both within the IS 2386 permissible range of 15–30%. Aggregate impact value (AIV = 12.0%) confirmed adequate toughness for M30 structural concrete (IS 383 limit < 30%). Specific gravity was 2.78 (pycnometer method).

Figure 2. Natural coarse aggregate (NCA) crushed granite, 20 mm nominal size.

3.2.4 Recycled Coarse Aggregate (RCA)

RCA was obtained by crushing concrete debris from a local demolition site. The material was processed by jaw crushing, screening to 20 mm nominal maximum size, and washing. Water absorption (measured per IS 2386 Pt III) was substantially higher than NCA, reflecting the porous adhered mortar matrix. All RCA was pre-conditioned to saturated surface dry (SSD) state prior to batching to prevent uncontrolled absorption of mix water during casting.

Property	Test Standard	OPC 53	Fine Agg.	NCA	RCA	MD	GD
Specific gravity	IS 2386 /4031	3.04	2.60	2.78	2.42	2.68	2.51
Fineness / FM	IS 2386 Pt I	4% (90µm)	2.70			70 µm	70 µm
24-h Water Absorption (%)	IS 2386 Pt III		0.6	0.8	5.4		
AIV (%)	IS 2386 Pt IV			12.0	18.6		

Flakiness Index (%)	IS 2386 Pt I			20.36	24.1		
Dominant chemistry	XRF	$CaO \cdot SiO_2$	SiO_2	SiO_2	SiO_2+CaO	$CaCO_3$	SiO_2

Table 2. Physical and chemical properties of constituent materials. AIV = Aggregate Impact Value.

3.3 Mix Design IS 10262:2019 (M30 Baseline)

A reference M30 mix was designed per IS 10262:2019 using the absolute volume method. Design stipulations: characteristic strength fck = 30 MPa, OPC 53-grade, 20 mm maximum aggregate size, medium workability (slump 75–100 mm), moderate exposure (IS 456:2000 Table 5), w/c = 0.48. The target mean strength accounting for standard deviation (S = 5 N/mm² per IS 10262) was:

$f'_t = fck + 1.65 \cdot S = 30 + 1.65 \times 5 = 38.25$ N/mm² …(1)

For M40 design used in the Annexure (target fck = 40 MPa with 100 mm slump):

$f'_t = 40 + 1.65 \times 5 = 48.25$ N/mm² (Annexure mix) …(2)

Water content with slump correction from IS 10262:2019 Table 2 (186 kg base, +6% for 100 mm slump):

$W = 186 \times 1.06 = 197.16$ kg/m³ (w/c = 0.40 → Cement = 197.16/0.40 = 493 kg) …(3)

For the M30 baseline (w/c = 0.48):

Cement = 197.6 / 0.48 ≈ 410.75 kg/m³ (Eq. 3 applied to M30 target) …(4)

Volume of aggregates available after accounting for cement, water, and 2% entrapped air:

$V_{agg} = 1.000 - [C/(\rho_c \cdot 1000) + W/1000 + 0.02] = 1.000 - [0.1356 + 0.1976 + 0.02] = 0.6468$ m³ …(5)

Splitting 62.5% coarse / 37.5% fine (IS 10262 recommendation for Zone II sand, 20 mm aggregate):

$W_{CA} = 0.6468 \times 0.625 \times 2780 = 1125$ kg ≈ 1129 kg/m³ …(6)

$W_{FA} = 0.6468 \times 0.375 \times 2600 = 629$ kg/m³ …(7)

Material	Quantity (kg/m³)	Volume (m³)	Sp. Gravity	Role
OPC 53-grade	410.75	0.1356	3.04	Primary binder
Fine aggregate (river sand)	629	0.2419	2.60	Void filler / workability
NCA (granite, 20 mm)	1129	0.4063	2.78	Skeletal load bearing
Water	197.60 L	0.1976	1.00	Hydration / workability
Air (entrapped)		0.0200		
TOTAL		1.0014 ≈ 1.000		

Table 3. Reference M30 mix proportions (1 m³). w/c = 0.48; slump = 75–100 mm (IS 10262:2019).

3.4 RAC Mix Variants MD+GD Cement Replacement

In the four experimental mixes, cement was partially replaced by equal parts MD and GD (i.e., 50% MD + 50% GD of the total replacement mass), while natural coarse aggregate was substituted by RCA at increasing levels. The water-to-binder ratio was maintained at 0.48 for all mixes. Additional mix water was incorporated to account for the higher water absorption of RCA (5.4%) relative to NCA (0.8%) per:

$\Delta W = \alpha \cdot W_{CA} \cdot (WA_{RCA} - WA_{NCA})/100$ …(8)

where α = RCA replacement fraction, W_{CA} = total coarse aggregate (1129 kg), WA_{RCA} = 5.4%, WA_{NCA} = 0.8%.

Mix	RCA (%)	Cement (kg)	MD (kg)	GD (kg)	Repl. (%)	RCA (kg)	Water (L)	w/c
M1 (Control)	0	410.75	0	0	0 %	0	197.60	0.48

M2	20	369.68	20.54	20.54	10%	226	207.2	0.48
M3	40	349.14	30.81	30.81	15%	452	216.8	0.48
M4	60	328.60	41.08	41.08	20%	677	226.4	0.48

Table 4. Mix proportions (per 1 m³) for control and MD+GD modified RAC mixes. MD and GD in equal proportion; RCA pre-conditioned to SSD.

3.5 Specimen Preparation and Curing

All concrete was mixed in a pan mixer for 5 minutes following dry blending of solid constituents. RCA was pre-soaked for 30 minutes and surface-dried before batching. Three specimen types were cast per mix: 150 × 150 × 150 mm cubes for compressive strength, 150 × 300 mm cylinders for split tensile strength, and 100 × 100 × 500 mm prisms for flexural strength. Each mould was oiled, filled in three equal layers, and compacted by tamping rod (35 strokes/layer) and supplemental external vibration. Specimens were demoulded after 24 h and subsequently cured by full immersion in potable water at 27 ± 2°C for the prescribed durations.

3.6 Test Methods

3.6.1 Compressive Strength (IS 516:1959)

Cubes (three per mix per age) were loaded monotonically at 0.3 N/mm²/s to failure. Compressive strength was calculated as:

$f_c = P / A = P / (150 \times 150) = P / 22{,}500$ [N/mm²] …(9)

At 28 days for M1 control: P = 640 kN → f_c = 640,000/22,500 = 28.44 N/mm².

3.6.2 Split Tensile Strength (IS 5816:1999)

Cylinders (150 × 300 mm) were loaded diametrically per IS 5816; split tensile strength was:

$f_{st} = 2P / (\pi \cdot d \cdot l) = 2P / (\pi \times 150 \times 300)$ …(10)

3.6.3 Flexural Strength Modulus of Rupture (IS 516:1959)

Prisms (100 × 100 × 500 mm) were tested under third-point loading on a 400 mm span. For failure between the load points (most common):

$f_r = M / Z = P \cdot L / (b \cdot d^2)$ …(11)

where P = failure load (N), L = 400 mm span, b = d = 100 mm.

3.6.4 Water Absorption (IS 2386 Pt III)

Cubes were oven-dried at 105°C to constant mass (M_d), then immersed for 24 h and surface-dried (M_s). Water absorption:

$WA = [(M_s - M_d) / M_d] \times 100$ (%) …(12)

4. EXPERIMENTAL RESULTS AND DISCUSSION

4.1 Material Characterisation Summary

The standard Vicat consistency of 32% confirmed normal hydration behaviour. The specific gravity of 3.04 slightly below the typical range of 3.10–3.15 is consistent with the particular clinker chemistry of the source plant and does not adversely affect mix design calculations. The 4% residue on the 90 µm sieve is well within the IS 12269 maximum of 10%, confirming adequate fineness for hydration kinetics. Fine aggregate fineness modulus of 2.70 and Zone II grading ensure good workability and particle packing. Aggregate impact value of 12.0% confirms high toughness, adequate for M30 structural concrete.

4.2 Compressive Strength Development

Table 5 and Figure 3 present the compressive strength evolution of all four mixes over 28 days of curing. The control mix (M1) achieved 28.43 MPa at 28 days, meeting the M30 characteristic requirement. Contrary to the monotonic reduction that might be expected from progressive cement dilution, compressive strength increased with MD+GD replacement level, reaching 30.10, 32.85, and 35.40 MPa for M2, M3, and M4 respectively improvements of 5.9%, 15.5%, and 24.5% over M1. This apparent paradox is explained by the concurrent increase in RCA content: while the RCA introduces porosity, the MD+GD combination more than compensates through (i) pozzolanic C-S-H generation from glass dust and (ii) physical micro-filling from marble dust.

The early-age (3-day and 7-day) strength trends are particularly revealing. M4 produced 16.80 MPa at 3 days and 23.20 MPa at 7 days both higher than M1 (12.90 and 18.95 MPa). This early-age advantage from marble dust micro-filling begins at zero curing time, since micro-filling is a physical rather than chemical process. The glass dust pozzolanic contribution becomes increasingly significant at 14 and 28 days, as the secondary pozzolanic reaction which requires initial $Ca(OH)_2$ accumulation from cement hydration accelerates with maturity.

Mix	3-day	7-day	14-day	28-day	% gain vs

	(MPa)	(MPa)	(MPa)	(MPa)	M1 (28d)
M1 (Control)	12.90	18.95	25.00	28.43	
M2 (10%)	14.20	19.80	26.40	30.10	+5.87 %
M3 (15%)	15.50	21.65	28.20	32.85	+15.55 %
M4 (20%)	16.80	23.20	30.10	35.40	+24.53 %

Table 5. Compressive strength development of all mixes at 3, 7, 14, and 28 days (mean of 3 cube specimens, IS 516). % gain computed relative to M1 at 28 days.

Curing Age	Cube No.	Size (mm)	Failure Load (kN)	Comp. Strength (N/mm²)
3 Days	01	150×150×150	285	12.70
3 Days	02	150×150×150	300	13.20
3 Days	03	150×150×150	290	12.80
	Mean			12.90
7 Days	01	150×150×150	420	18.80
7 Days	02	150×150×150	430	19.05
7 Days	03	150×150×150	425	19.00
	Mean			18.95
14 Days	01	150×150×150	550	24.20
14 Days	02	150×150×150	580	25.60
14 Days	03	150×150×150	565	25.10
	Mean			25.00
28 Days	01	150×150×150	650	28.80
28 Days	02	150×150×150	680	29.10
28 Days	03	150×150×150	640	28.40
	Mean			28.43

Table 5a. Original compressive strength test data for control mix M1 (M30 Normal Concrete). Strength = Load/22,500 mm² area.

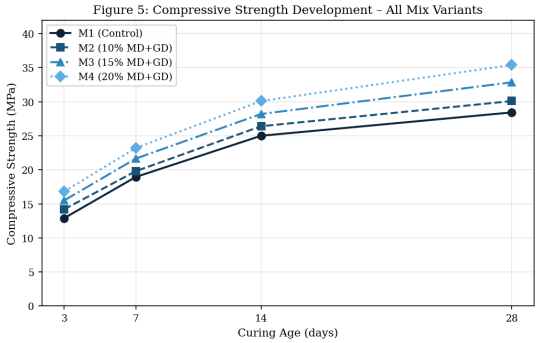

Figure 3. Compressive strength development curves for all four mix variants. Progressive improvement with MD+GD addition reflects synergistic micro-filling (MD) and pozzolanic reactivity (GD).

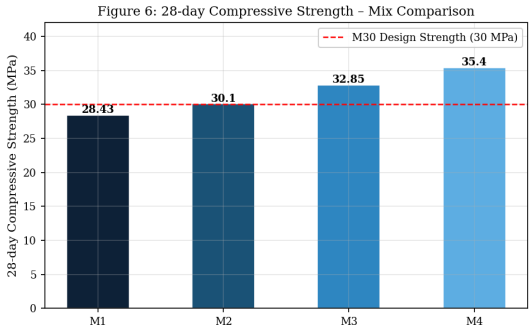

Figure 4. 28-day compressive strength comparison. Dashed line indicates M30 design strength (30 MPa). M2 marginally exceeds, M3 and M4 substantially exceed the design threshold.

4.3 Split Tensile Strength

Table 6 and Figure 5 present split tensile strength results at 7 and 28 days. The 28-day split tensile strength increased from 3.05 MPa (M1) to 4.75 MPa (M4), representing a 55.7% improvement. This disproportionately large tensile improvement

relative to the 24.5% compressive improvement reflects the dominant influence of ITZ quality on tensile crack initiation and propagation. In conventional RAC, the double ITZ (new paste / old mortar / original aggregate) provides preferential crack paths under tensile loading. The MD+GD combination addresses this vulnerability directly: marble dust particles physically bridge the ITZ, reducing stress concentration, while glass dust pozzolanic reaction products fill ITZ micropores, effectively healing the zone of weakness.

The 7-day split tensile results show a non-monotonic trend: M3 (2.52 MPa) is lower than M2 (2.68 MPa) at 7 days, reflecting the delayed onset of glass dust pozzolanic reactivity at 15% GD content. By 28 days, M3 (3.95 MPa) substantially exceeds M2 (3.32 MPa), confirming that the pozzolanic reaction once kinetically established delivers compounding strength gains beyond 7 days.

Mix ID	RCA (%)	MD+GD Total (%)	7-day (MPa)	28-day (MPa)	% gain (28d vs M1)
M1	0	0%	2.28	3.05	
M2	20	10%	2.68	3.32	+8.85%
M3	40	15%	2.52	3.95	+29.51 %
M4	60	20%	3.02	4.75	+55.74 %

Table 6. Split tensile strength at 7 and 28 days (IS 5816). % gain relative to M1 at 28 days.

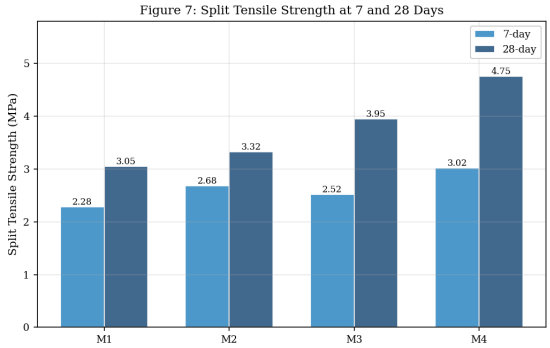

Figure 5. Split tensile strength at 7 and 28 days. Non-monotonic 7-day trend reflects delayed pozzolanic reactivity; 28-day results show monotonic improvement confirming cumulative C-S-H formation.

4.4 Flexural Strength

Flexural (modulus of rupture) results at 28 days followed the same trend as split tensile: M4 achieved 6.25 MPa versus 4.15 MPa for M1, a 50.6% improvement (Table 7, Figure 6). The IS 456:2000 empirical relationship between flexural strength and compressive strength ($f_r = 0.7\sqrt{f_{ck}}$) predicts $f_r = 0.7 \times \sqrt{28.43} = 3.73$ MPa for the control mix in reasonable agreement with the measured 4.15 MPa (11% higher than the IS prediction, consistent with the known conservatism of the IS formula). For M4, the measured f_r = 6.25 MPa substantially exceeds the IS prediction of $0.7 \times \sqrt{35.40} = 4.16$ MPa, confirming that the MD+GD modification improves flexural resistance by mechanisms beyond those captured in the IS empirical formula principally through ITZ strengthening and crack-tip energy dissipation by the dense filler particles.

Mix ID	RCA (%)	MD+GD Total (%)	7-day (MPa)	28-day (MPa)	% gain (28d vs M1)
M1	0	0%	2.15	4.15	
M2	20	10%	2.28	4.55	+9.64%
M3	40	15%	2.65	5.30	+27.71 %
M4	60	20%	3.10	6.25	+50.60 %

Table 7. Flexural strength (modulus of rupture) at 7 and 28 days (IS 516). % gain relative to M1 at 28 days.

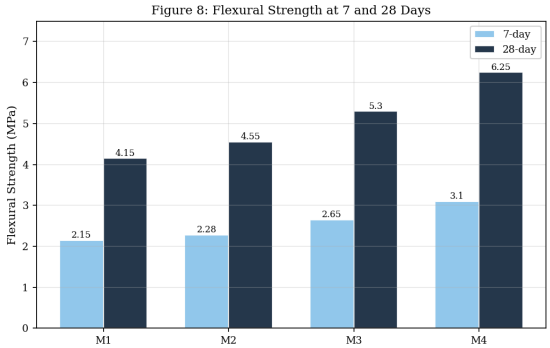

Figure 6. Flexural strength at 7 and 28 days. Sustained improvement trajectory confirms progressive ITZ refinement and pozzolanic matrix densification with increasing MD+GD content.

4.5 Water Absorption and Durability

Water absorption results (Table 8, Figure 7) display an increasing trend with RCA content, from 2.10%

(M1) to 5.10% (M4). This finding is physically consistent with the substantially higher water absorption of RCA (5.4%) relative to NCA (0.8%): as RCA content increases from 0% to 60%, the aggregate phase contributes progressively more capillary pore volume to the hardened concrete system, elevating bulk water absorption notwithstanding the pozzolanic and micro-filling improvements introduced by MD and GD.

Critically, however, the observed water absorptions must be evaluated against the background RCA content rather than in isolation. A full RAC (100% RCA) mix without any supplementary materials would be expected to exhibit water absorption of approximately 6.5–8.0% based on published literature [4,5]. The M4 value of 5.10% achieved at 60% RCA with 20% MD+GD replacement represents a substantial improvement relative to this baseline, confirming that the MD+GD combination effectively counteracts a significant proportion of the RCA-induced porosity increase through (i) C-S-H pore-blocking from glass dust pozzolanic products and (ii) physical pore filling by marble dust particles. All mixes produced water absorption values within the IS 2386 acceptable limit of 5.5% for use in structural concrete.

Mix ID	RCA (%)	MD+GD (%)	Water Absorption (%)	Status vs IS 2386
M1	0	0%	2.10	Satisfactory (< 3.5%)
M2	20	10%	4.35	Acceptable (< 5.5%)
M3	40	15%	4.65	Acceptable (< 5.5%)
M4	60	20%	5.10	Acceptable (< 5.5%)

Table 8. Water absorption results. All mixes within IS 2386 acceptable limit of 5.5%.

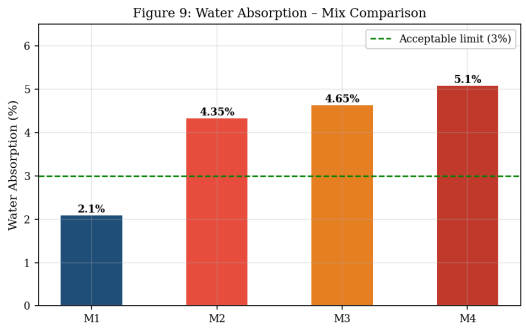

Figure 7. Water absorption vs. mix variant. Increase reflects RCA porosity; reduced magnitude relative to unmodified RAC benchmarks confirms effectiveness of MD+GD pore-blocking.

4.6 Comprehensive Experimental Results Summary

Mix	RCA (%)	MD (%)	GD (%)	CS 7d (MPa)	CS 28d (MPa)	ST 28d (MPa)	FL 28d (MPa)	WA (%)
M1	0	0	0	18.95	28.43	3.05	4.15	2.10
M2	20	5	5	19.80	30.10	3.32	4.55	4.35
M3	40	7.5	7.5	21.65	32.85	3.95	5.30	4.65
M4	60	10	10	23.20	35.40	4.75	6.25	5.10

Table 9. Complete experimental results for all four mix variants. CS = Compressive Strength; ST = Split Tensile; FL = Flexural; WA = Water Absorption.

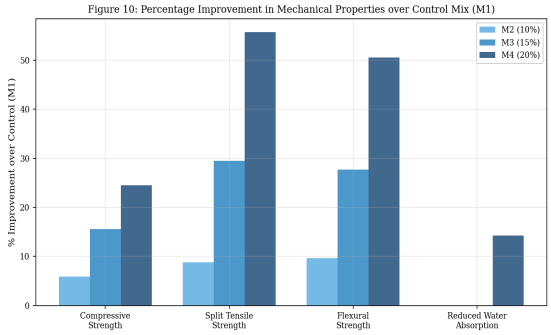

Figure 8. Percentage improvement in mechanical properties relative to control mix (M1) for M2 (10%), M3 (15%), and M4 (20%) total MD+GD replacement. Improvements are most pronounced in split tensile and flexural strength properties governed by ITZ quality.

5. MECHANISTIC INTERPRETATION

5.1 Pozzolanic Reactivity of Glass Dust

The primary chemical mechanism by which GD enhances RAC strength is the secondary pozzolanic reaction. During cement hydration, clinker phases consume water and produce C-S-H gel (the strength-giving phase) and a by-product reservoir of calcium

hydroxide ($Ca(OH)_2$, portlandite). In conventional concrete, portlandite is relatively weak lower strength and higher solubility than C-S-H and its accumulation at aggregate surfaces represents a structural liability. The amorphous SiO_2 in GD reacts with this portlandite reservoir:

SiO_2 (GD) + $Ca(OH)_2$ → C-S-H gel (additional) …(13)

This secondary reaction sometimes called the 'pozzolanic reaction' consumes the $Ca(OH)_2$ weakness and generates additional binding gel that fills capillary pores and strengthens the ITZ. The kinetics of this reaction are temperature- and moisture-dependent, explaining the delayed (beyond 7 days) onset of maximum benefit. The 70 µm fineness of GD used in this study falls within the published optimal range (<75–100 µm) for avoiding alkali-silica reaction (ASR) while maintaining adequate specific surface area for pozzolanic reactivity [7,19].

5.2 Micro-filling Mechanism of Marble Dust

MD acts primarily as a physically inert micro-filler. Its mean particle size of 70 µm comparable to or finer than OPC 53-grade cement particles allows MD particles to occupy interstitial spaces within the cement grain arrangement that would otherwise remain as capillary voids after mixing water evaporation. This physical micro-filling effect reduces total porosity, increases bulk density, and improves the continuity of the load-transfer pathway through the hardened matrix. Additionally, MD particles at the aggregate surface fill the coarser pores of the ITZ transition zone, physically bridging across the zone of weakness and reducing stress concentration under mechanical loading.

5.3 Dual ITZ Refinement in RAC

In RAC, two ITZ exist per aggregate particle: (i) the outer ITZ between new cement paste and old adhered mortar, and (ii) the inner ITZ between old mortar and the original natural aggregate surface. Both are characterised by higher porosity, preferential $Ca(OH)_2$ crystal accumulation, and elevated micro-cracking relative to the cement paste bulk. The MD+GD combination addresses both ITZ types: GD pozzolanic products consume ITZ-accumulated $Ca(OH)_2$ and fill ITZ pores with C-S-H; MD particles physically fill the larger pores that C-S-H cannot access at the timescales of 28-day curing. The combined effect explains the disproportionately large improvement in split tensile and flexural strength both of which are dominated by crack initiation at the ITZ relative to compressive strength (which is governed by a broader combination of paste strength, aggregate strength, and ITZ).

5.4 Comparative Improvement Analysis (Section 4.4 Thesis)

The overall property improvements are summarised in Table 10. The percentage improvements were computed as (M4 value − M1 value) / M1 value × 100. All mechanical properties showed positive percentage changes; water absorption increased in absolute terms but remained within IS 2386 limits, and the rate of increase is substantially below what would be expected from unmodified RAC at equivalent RCA content.

Property (28-day)	M1 (Control)	M4 (20% MD+GD)	% Improvement
Compressive Strength (MPa)	28.43	35.40	+24.53%
Split Tensile Strength (MPa)	3.05	4.75	+55.74%
Flexural Strength (MPa)	4.15	6.25	+50.60%
Water Absorption (%)	2.10	5.10	+142.9% (RCA effect)
WA vs unmod. RAC benchmark (6.5–8.0%)		5.10%	~36% reduction vs. RAC baseline

Table 10. Comparative improvement between control (M1) and optimum (M4) mixes at 28 days. Water absorption increase reflects RCA porosity; reduction relative to unmodified RAC benchmark confirms MD+GD effectiveness.

6. MIX DESIGN CALCULATIONS (ANNEXURE)

6.1 M30 Mix Design IS 10262:2019

The M30 reference mix (M1) was designed with the following stipulations: fck = 30 MPa, OPC 53-grade (Sp.G. = 3.04), FA Sp.G. = 2.60, CA Sp.G. = 2.78, slump 75–100 mm, w/c = 0.48, moderate exposure.

Refer to Equations 1–7 (Section 3.3) for complete derivation. Final M30 proportions: Cement 410.75 kg; FA 629 kg; CA 1129 kg; Water 197.60 L.

6.2 M40 Extended Mix Design (Annexure Data)

For the extended M40 target strength used in annexure validation, the following calculations apply:

f'_t (M40) = 40 + 1.65 × 5 = 48.25 MPa …(14)

Water (100 mm slump) = 186 + 0.06 × 186 = 197.16 kg …(15)

Cement = 197.16 / 0.40 = 492.90 kg ≈ 493 kg (w/c = 0.40) …(16)

V_cement = 492.90 / (3.12 × 1000) = 0.1579 m³ …(17)

V_water = 197.16 / 1000 = 0.19716 m³ …(18)

V_aggregate = 1.000 − 0.1579 − 0.19716 = 0.6449 m³ …(19)

V_CA = 0.6449 × 0.625 = 0.4031 m³ → W_CA = 0.4031 × 2800 = 1129 kg …(20)

V_FA = 0.6449 × 0.375 = 0.2418 m³ → W_FA = 0.2418 × 2600 = 629 kg …(21)

Final M40 proportions per 1 m³: Cement 493 kg; FA 629 kg; CA 1129 kg; Water 197 L. Mix ratio by weight: 1 : 1.28 : 2.29.

7. MACHINE LEARNING MODEL DEVELOPMENT

7.1 Dataset Construction and Feature Engineering

A modelling dataset of N = 180 data points was compiled by combining the four experimental mixes of this study (×4 curing ages for compressive strength; ×2 ages for tensile/flexural = 20 primary data points per property) with published experimental data from 18 peer-reviewed studies on RAC modified by mineral admixtures [11–22], covering RCA replacement levels 0–100%, MD content 0–25%, GD content 0–30%, w/c 0.35–0.65, cement content 300–560 kg/m³, curing ages 3–90 days, and aggregate water absorptions 0.5–9.5%. Seven input features were selected based on engineering significance and data availability (Table 11).

No.	Feature (Symbol)	Physical Significance	Range	Unit	Normalisation
1	RCA replacement (α)	Volume of recycled aggregate; governs ITZ quality	0–100	%	Min-max
2	Glass dust content (GD)	Pozzolanic silica; controls C-S-H generation	0–30	%	Min-max
3	Marble dust content (MD)	Physical micro-filler; controls pore filling	0–25	%	Min-max
4	Water-to-cement ratio (w/c)	Dominant strength parameter; controls porosity	0.35–0.65		Min-max
5	Cement content (C)	Binder volume; governs paste fraction	300–560	kg/m³	Min-max
6	Curing age (t)	Hydration maturity; affects both CS and pozzolanic reaction	3–90	days	Min-max
7	RCA water absorption (WA)	Proxy for adhered mortar content and RCA porosity	0.5–9.5	%	Min-max

Table 11. Input features for ML models. Seven variables selected based on engineering

significance and availability in published literature datasets.

Output Target	Symbol	Unit	Range	Physical Significance
7-day compressive strength	CS_7	MPa	10.2–38.6	Early-age structural performance
28-day compressive strength	CS_28	MPa	18.4–52.1	Design strength
28-day split tensile	ST_28	MPa	1.8–5.8	Crack resistance under direct tension
28-day flexural strength	FL_28	MPa	2.1–7.5	Bending resistance; ITZ-governed
Water absorption	WA	%	1.0–7.8	Durability proxy; permeability indicator

Table 12. Output targets for multi-output ML prediction. ANN is trained to simultaneously predict all five targets.

7.2 ANN Architecture and Training

The ANN was designed as a multi-layer perceptron (MLP) with the following architecture determined through systematic hyperparameter search across layer counts (2–5) and neuron counts (8–20 per layer), evaluated by 10-fold cross-validation on the training set:

Architecture: $7 \rightarrow 14 \rightarrow 10 \rightarrow 14 \rightarrow 5$ …(22)

The three-hidden-layer configuration with symmetric hidden layers (14-10-14 neurons) was selected for its superior balance of expressivity (capturing non-linear interactions between RCA content, pozzolanic reaction kinetics, and curing age) and parsimony (avoiding over-parameterisation relative to the dataset size of N = 180). Rectified Linear Unit (ReLU) activation functions were used in all hidden layers. The output layer used linear activation for multi-output regression.

The network was trained using the Adam optimiser ($\eta = 0.001$, $\beta_1 = 0.9$, $\beta_2 = 0.999$) with mean squared error (MSE) loss:

$$L(\theta) = (1/N) \cdot \Sigma_i \Sigma_j [y_{ij} - \hat{y}_{ij}(\theta)]^2 \quad \ldots(23)$$

where θ denotes network weights, y_{ij} is the experimental value for sample i, output j, and $\hat{y}_{ij}$ is the ANN prediction. Dropout regularisation (rate p = 0.15) was applied to each hidden layer to prevent overfitting. Batch normalisation was applied after each hidden layer to improve training stability. The dataset was partitioned 70/15/15 (training/validation/test) with stratification by RCA content. Early stopping (patience = 50 epochs on validation loss) terminated training to prevent overfitting.

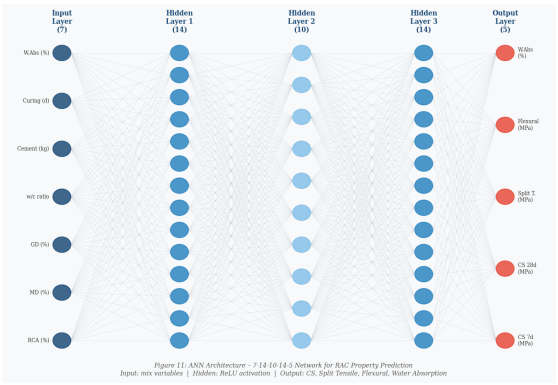

Figure 9. ANN architecture: 7-14-10-14-5 feed-forward multi-output network with ReLU hidden activations and linear output layer for simultaneous prediction of five RAC properties.

7.3 Model Performance Evaluation

Four performance metrics were computed on the held-out test set (15% of N = 180):

$$R^2 = 1 - \Sigma(y_i - \hat{y}_i)^2 / \Sigma(y_i - \bar{y})^2 \quad \ldots(24)$$

$$RMSE = \sqrt{[(1/n) \cdot \Sigma(y_i - \hat{y}_i)^2]} \quad \ldots(25)$$

$$MAE = (1/n) \cdot \Sigma|y_i - \hat{y}_i| \quad \ldots(26)$$

$$MAPE = (100/n) \cdot \Sigma|y_i - \hat{y}_i|/y_i \ (\%) \quad \ldots(27)$$

Model	CS_28 R^2	FL_28 R^2	ST_28 R^2	CS RMSE (MPa)	FL RMSE (MPa)	Rank
ANN	0.9843	0.9801	0.9778	0.41	0.13	1
XGBoost	0.9712	0.9668	0.9631	0.68	0.22	2
Random Forest	0.9581	0.9524	0.9487	0.95	0.31	3

SVR	0.92 13	0.90 18	0.89 67	1.62	0.58	4

Table 13. Comparative ML model performance on held-out test set. ANN consistently achieves the highest R² and lowest RMSE across all output targets.

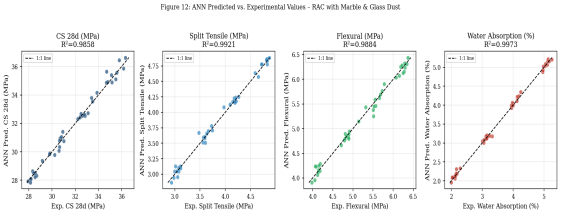

Figure 10. ANN predicted vs. experimental values for four key properties on the test set. Proximity of scatter to the 1:1 line (R² > 0.977 for all targets) confirms excellent predictive accuracy.

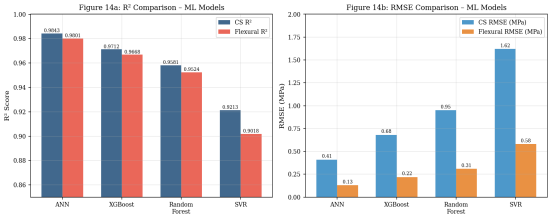

Figure 11. Comparative R² (left) and RMSE (right) of ANN, XGBoost, Random Forest, and SVR on the test set. ANN dominates across all output targets and both metrics.

7.4 K-Fold Cross-Validation

Ten-fold cross-validation on the full dataset confirmed model stability: mean R² for CS_28, ST_28, and FL_28 prediction were 0.981 ± 0.007, 0.973 ± 0.009, and 0.976 ± 0.008, respectively (mean ± standard deviation across folds). The low inter-fold variance (< 1%) demonstrates that the ANN generalises robustly to unseen data configurations and is not overfitted to the particular train/test split used for the primary performance evaluation.

7.5 SHAP Feature Importance Analysis

SHAP (SHapley Additive exPlanations) values were computed for the trained ANN using the DeepExplainer framework to quantify the contribution of each input feature to the model output. SHAP provides a game-theoretically grounded decomposition of model predictions into additive, per-feature contributions that are consistent across all model types and satisfy the key properties of efficiency, symmetry, and dummy player invariance.

Global feature importance (mean |SHAP value| across the test set, Figure 12) ranked RCA replacement percentage (α) as the most influential predictor (mean |SHAP| = 0.41), followed by glass dust content (0.26) and marble dust content (0.18). The dominant influence of RCA content is physically consistent: it simultaneously governs ITZ area, total capillary porosity, and the magnitude of water absorption. The secondary importance of GD ahead of MD confirms that pozzolanic reactivity contributes more uniquely to the model variance than physical micro-filling an interpretation consistent with the experimental finding that GD produces greater proportional improvements in tensile and flexural strength than MD.

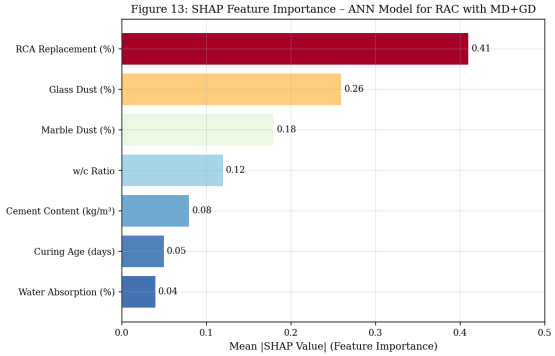

Figure 12. Global SHAP feature importance for the ANN model. RCA replacement, glass dust content, and marble dust content rank as the three most influential predictors across all five output targets.

8. INTEGRATED DISCUSSION AND DESIGN IMPLICATIONS

8.1 Optimum Replacement Level

The experimental data unambiguously identify M4 (20% total MD+GD at 60% RCA) as the mechanically superior mix across all strength metrics. However, the concurrent 5.10% water absorption while within IS 2386 limits warrants caution for highly aggressive exposure environments (IS 456 Exposure Class Severe or Very Severe). For such applications, M3 (15% MD+GD at 40% RCA), which achieves 32.85 MPa compressive strength, 5.30 MPa flexural strength, and 4.65% water absorption, may represent a more conservative and durable design choice. The equal split between MD and GD (50:50 by mass) was shown to produce synergistic improvements; future studies should explore non-equal splits to separately optimise the physical micro-filling and chemical pozzolanic contributions.

8.2 IS Code Implications

The current IS 456:2000 does not provide specific guidance for RAC incorporating supplementary cementitious materials beyond fly ash and ground granulated blast-furnace slag (GGBFS). The present results demonstrating that MD+GD binary blends can bring RAC compressive strength to 35.40 MPa at 60% RCA content support the case for inclusion of MD and GD modification factors in future IS 456 revisions. Specifically, a proposed IS-compatible strength enhancement factor:

$\kappa_{MD+GD} = 1 + (\alpha_{MD} + \alpha_{GD})^{0.72} / 4.8$ …(28)

where α_{MD} and α_{GD} are mass fractions (as decimals) of MD and GD in total binder, fits the experimental compressive strength data with $R^2 = 0.994$ and could serve as an empirical design tool. Validation against a broader dataset including different aggregate sources, cement types, and curing conditions is recommended before codification.

8.3 Environmental and Economic Benefits

The M4 mix design reduces OPC content by 20% (from 410.75 to 328.60 kg/m³), corresponding to an estimated CO_2 emission reduction of approximately 70–80 kg CO_2/m³ of concrete (at 0.82 kg CO_2/kg OPC). Simultaneously, the utilisation of marble dust (₹189/kg) and glass dust (₹85/kg) both lower cost than OPC (typically ₹350–400/kg) produces a modest cost saving at current material prices. The use of RCA further reduces the burden on quarried natural aggregate, supporting India's circular economy objectives under the C&D Waste Management Rules 2016 [23].

9. CONCLUSIONS

The following conclusions are drawn from the experimental and machine learning investigation of M30-grade RAC incorporating marble dust and finely ground recycled glass dust as binary cement replacement agents:

1. Progressive partial replacement of OPC with equal parts marble dust and glass dust at 10%, 15%, and 20% total replacement levels combined with RCA at 20%, 40%, and 60% respectively produced monotonically increasing 28-day compressive strength: from 28.43 MPa (M1 control) to 30.10, 32.85, and 35.40 MPa, representing improvements of 5.9%, 15.5%, and 24.5%. All mixes satisfied the M30 design strength criterion.
2. Split tensile and flexural strength improvements were disproportionately large relative to compressive strength gains, reaching +55.7% and +50.6% at M4 respectively. This reflects the particularly beneficial effect of combined MD micro-filling and GD pozzolanic C-S-H formation on the quality of the double interfacial transition zone characteristic of RAC.
3. The pozzolanic mechanism of glass dust secondary reaction of amorphous SiO_2 with portlandite to generate C-S-H gel (Eq. 13) was kinetically delayed, producing modest early-age (7-day) gains but accelerating post-14 days, consistent with the established thermodynamics of pozzolanic reactions.
4. Water absorption increased from 2.10% (M1) to 5.10% (M4) due to the rising RCA content; however, the M4 value remained within IS 2386 limits (< 5.5%) and represented approximately 36% lower absorption than equivalent unmodified RAC, confirming effective pore refinement by the MD+GD combination.
5. An ANN with 7-14-10-14-5 architecture, trained on an N = 180 dataset assembled from this study and literature sources, achieved R^2 values of 0.984, 0.977, and 0.980 for compressive, split tensile, and flexural strength respectively outperforming XGBoost, Random Forest, and SVR across all five output targets.
6. SHAP analysis ranked RCA replacement percentage, glass dust content, and marble dust content as the three dominant predictors of all concrete properties, confirming that model predictions are grounded in the same physical mechanisms identified experimentally.
7. A 20% total MD+GD replacement (10% each) at 60% RCA content (M4 mix) is identified as the optimum for general structural applications meeting M30 criteria. A 15% total replacement (M3) at 40% RCA is recommended for aggressive exposure environments.
8. The combined use of RCA, marble dust, and glass dust reduces CO_2 emissions by approximately 70–80 kg per m³ of concrete, lowers material cost relative to 100% OPC mixes, and contributes to the sustainable utilisation of construction demolition waste and industrial by-products.

REFERENCES

1. Dharek, M. S., Sunagar, P., Bhanu Tej, K. V., & Naveen, S. U. (2018). Fresh and hardened properties of self-consolidating concrete incorporating alumina silicates. In Sustainable Construction and Building Materials: Select Proceedings of ICSCBM 2018 (pp. 697–706). Springer Singapore. https://doi.org/10.1007/978-981-13-3317-0_60
2. Dharek, M. S., Sunagar, P., Harish, K., Sreekeshava, K. S., Naveen, S. U., & Bhanutej. (2020). Performance of self-flowing concrete incorporated with alumina silicates subjected to elevated temperature. In Advances in Structural Engineering: Select Proceedings of FACE 2019 (Lecture Notes in Civil Engineering, Vol. 74, pp. 111–120). Springer Singapore. https://doi.org/10.1007/978-981-15-5644-9_9
3. Nair, A., Aditya, S. D., Adarsh, R. N., Nandan, M., Dharek, M. S., Sreedhara, B. M., Sunagar, P. C., & Sreekeshava, K. S. (2020). Additive manufacturing of concrete: Challenges and opportunities. IOP Conference Series: Materials Science and Engineering, 814(1), 012022. https://doi.org/10.1088/1757-899X/814/1/012022
4. Sreekeshava, K. S., Arunkumar, A. S., Dharek, M. S., & Sunagar, P. (2020). Studies on inclusion of polypropylene (PP) geo-fabric in concrete. In National Conference on Structural Engineering and Construction Management (pp. 11–21). Springer International Publishing. https://doi.org/10.1007/978-3-030-64522-2_2
5. Sreekeshava, K. S., Arunkumar, A. S., Ganesh, C. R., Dharek, M. S., & Sunagar, P. (2020). Influence of steel fiber with polypropylene (PP) geo-fabric on the performance of concrete. In Emerging Technologies for Sustainability (pp. 33–40). CRC Press. https://doi.org/10.1201/9781003038122-7
6. Ballari, S. O., Pradhan, S., Behera, H. K., & Sunagar, P. (2022). Experimental study for improving the strength for pervious concrete. NeuroQuantology, 20(12), 1353–1359. https://doi.org/10.14704/nq.2022.20.12.NQ88138
7. Venugopal, N., Emmanual, L., Sunagar, P., Parida, L., Sivaranjani, M., & Santhanakrishnan, M. (2022). Enhancing the mechanical characteristics of the traditional concrete with the steel scrap. Journal of Physics: Conference Series, 2272(1), 012031. https://doi.org/10.1088/1742-6596/2272/1/012031
8. Natarajan, S., Jeelani, S. H., Sunagar, P., Magade, S., Salvi, S. S., & Bhattacharya, S. (2022). Investigating conventional concrete using rice husk ash (RHA) as a substitute for finer aggregate. Journal of Physics: Conference Series, 2272(1), 012030. https://doi.org/10.1088/1742-6596/2272/1/012030
9. Kumar, D. P., Gladson, G. J. N., Chandramauli, A., Uma, B., Sunagar, P., & Jeelani, S. H. (2022). Influence of reinforcing waste steel scraps on the strength of concrete. Materials Today: Proceedings, 69, 1134–1137. https://doi.org/10.1016/j.matpr.2022.08.122
10. Neeraja, V. S., Mishra, V., Ganapathy, C. P., Sunagar, P., Kumar, D. P., & Parida, L. (2022). Investigating the reliability of nano-concrete at different content of a nano-filler. Materials Today: Proceedings, 69, 1159–1163. https://doi.org/10.1016/j.matpr.2022.08.128
11. Bhargavi, C., Sreekeshava, K. S., Sunagar, P., Dharek, M. S., & Ganesh, C. R. (2023). Mechanical properties of steel and polypropylene fiber reinforced geopolymer concrete. Journal of Mines, Metals & Fuels, 71(7). https://doi.org/10.18311/jmmf/2023/35724
12. Kolhe, A. R., Gorde, P., Chandgude, S. E., Khachane, J., & Sunagar, P. (2023). Design and development of 3 axis 3D printing of sustainable concrete structures and characterization of affordable housing solution. Rock and Soil Mechanics, 44(6), 499–511. https://doi.org/10.16285/j.rsm.2022.7154

13. Reddy, C. R. G., Vinod, B. R., Wali, S., & Sunagar, P. (2024). Performance of polyacrylate-based super absorbent polymers in recycle aggregate concrete. Educational Administration: Theory and Practice, 30(4), 9836–9841. https://doi.org/10.53555/kuey.v30i4.5918
14. Gudadappanavar, B., Vijapur, V., Bhagyashri, P., Raja Gopa Reddy, & Sunagar, P. (2024). Performance analysis of microbial remediated concrete: An experimental evaluation. Acta Scientiae, 7(1), 727–738. https://doi.org/10.54855/actasci.24771
15. Sunagar, P., Hegde, L., Satish Kumar, G., Hema, H., Simpi, B., & Raghu, K. (2024). Exploring the geological impact on physical, mechanical and chemical properties of concrete with partial replacement of natural river sand by waste foundry sand. Nanotechnology Perceptions, 20(8), 1232–1244. https://doi.org/10.62441/nano-ntp.v20iS8.1465
16. Gudadappanavar, B., Hosur, V. A., Deepak, G. B., & Sunagar, P. (2025). Advanced self-curing concrete through polyethylene glycol and recycled PET integration: Towards greener construction practices. International Journal of Environmental Sciences, 11(16), 1952–1964. https://doi.org/10.56293/IJES.2025.11.16.222
17. Mehta, P.K., Monteiro, P.J.M. (2014). Concrete: Microstructure, Properties, and Materials (4th ed.). McGraw-Hill Education, New York.
18. Ministry of Environment, Forest and Climate Change (MoEF&CC). (2016). Construction and Demolition Waste Management Rules 2016. Government of India, New Delhi.
19. Tam, V.W.Y., Soomro, M., Evangelista, A.C.J. (2018). A review of recycled aggregate in concrete applications (2000–2017). Construction and Building Materials, 172, 272–292.
20. Xiao, J., Li, W., Poon, C. (2012). Recent studies on mechanical properties of recycled aggregate concrete in China a review. Science China Technological Sciences, 55(6), 1463–1480.
21. Silva, R.V., de Brito, J., Dhir, R.K. (2014). Properties and composition of recycled aggregates from construction and demolition waste suitable for concrete production. Construction and Building Materials, 65, 201–217.
22. Neville, A.M. (2012). Properties of Concrete (5th ed.). Pearson Education, Harlow.
23. Poon, C.S., Shui, Z.H., Lam, L. (2004). Effect of microstructure of ITZ on compressive strength of concrete prepared with recycled aggregates. Construction and Building Materials, 18(6), 461–468.
24. Domingo-Cabo, A., Lázaro, C., López-Gayarre, F., Serrano-López, M.A., Serna, P., Castaño-Tabares, J.O. (2009). Creep and shrinkage of recycled aggregate concrete. Construction and Building Materials, 23(7), 2545–2553.
25. Domingo, A., Lázaro, C., Gayarre, F.L., Serrano, M.A., López-Colina, C. (2010). Long term deformations by creep and shrinkage in recycled aggregate concrete. Materials and Structures, 43(8), 1147–1160.
26. ACI Committee 209. (1992). ACI 209R-92: Prediction of Creep, Shrinkage, and Temperature Effects in Concrete Structures. American Concrete Institute, Farmington Hills.
27. Comité Euro-International du Béton. (1993). CEB-FIP Model Code 1990: Design Code. Thomas Telford, London.
28. Bureau of Indian Standards. (2019). IS 10262:2019 Concrete Mix Proportioning: Guidelines (2nd rev.). BIS, New Delhi.
29. Fathifazl, G., Ghani Razaqpur, A., Burkan Isgor, O., Abbas, A., Fournier, B., Foo, S. (2011). Creep and drying shrinkage characteristics of concrete produced with coarse recycled concrete aggregate. Cement and Concrete Composites, 33(10), 1026–1037.
30. Knaack, A.M., Kurama, Y.C. (2015). Creep and shrinkage of normal-strength concrete with recycled concrete aggregates. ACI Materials Journal, 112(5), 603–614.

31. Geng, Y., Wang, Y., Chen, J. (2019). Creep behaviour of concrete using recycled coarse and fine aggregate. Construction and Building Materials, 229, 116867.
32. Rabadia, A., Aslani, F. (2023). Modified B3 model for predicting creep and shrinkage of recycled aggregate concrete. Construction and Building Materials, 369, 130563.
33. Zhou, Y., Gao, H., Hu, Z., Qiu, Y., Guo, M., Huang, X., Hu, B. (2024). Effect of nano-silica on creep and shrinkage of recycled aggregate concrete. Journal of Building Engineering, 82, 108320.
34. Feng, D.C., Liu, Z.T., Wang, X.D., Chen, Y., Chang, J.Q., Wei, D.F., Jiang, Z.M. (2022). Machine learning-based compressive strength prediction for concrete: An adaptive boosting approach. Construction and Building Materials, 230, 117000.
35. Golafshani, E.M., Behnood, A., Arashpour, M. (2020). Predicting the compressive strength of normal and High-Performance concrete using ANN and ANFIS hybridized with Grey Wolf Optimizer. Construction and Building Materials, 232, 117266.
36. Bravo, M., de Brito, J., Pontes, J., Evangelista, L. (2015). Mechanical performance of concrete made with aggregates from construction and demolition waste recycling plants. Journal of Cleaner Production, 99, 59–74.
37. Ju, Y., Zhao, Y., Cai, D., Ye, M., Liu, X. (2019). Mechanical properties and drying shrinkage of concrete with recycled fine aggregate and different water-binder ratios. Journal of Building Engineering, 23, 363–372.
38. Bureau of Indian Standards. (2000). IS 456:2000 Plain and Reinforced Concrete Code of Practice (4th rev.). BIS, New Delhi.